Electronic Supplementary Information

Gas-phase kinetics of CH_3CHO with OH radicals between 11.7 and 177.5 K

Sergio Blázquez,[a] Daniel González,[a] Elias M. Neeman,[a] Bernabé Ballesteros,[ab] Marcelino Agúndez,[c] André Canosa,[d] José Albaladejo,[ab] José Cernicharo,[c] and Elena Jiménez,*[ab]

[a] *Departamento de Química Física, Facultad de Ciencias y Tecnologías Químicas. Universidad de Castilla-La Mancha. Avda. Camilo José Cela 1B, 13071, Ciudad Real, Spain. E-mail: Elena.Jimenez@uclm.es*
[b] *Instituto de Investigación en Combustión y Contaminación Atmosférica (ICCA). Universidad de Castilla-La Mancha. Camino de Moledores s/n, 13071, Ciudad Real, Spain.*
[c] *Molecular Astrophysics Group, Instituto de Física Fundamental (IFF-CSIC). Consejo Superior de Investigaciones Científicas. C/ Serrano 123, 28006, Madrid, Spain.*
[d] *CNRS, IPR (Institut de Physique de Rennes)-UMR 6251. Université de Rennes, F-35000 Rennes, France*

Aerodynamic characterization of Laval nozzles: Pitot tube measurements of the impact pressure

The aerodynamic characterization of some of the employed nozzles was previously performed by using a Pitot tube. It consists of a fast pressure transducer (Kulite model XCQ-062) that measures the impact pressure (P_i) as a function of the distance from the exit of the nozzle.[1-8] Knowing P_i and the adiabatic expansion coefficient of the bath gas, the Mach number (M), T, n, P and hydrodynamic time (t_{hydro}) through the jet were calculated. An extended description of CRESU system was reported by Jiménez *et al*.[7] In this work, we present the aerodynamic characterization of 5 Laval nozzles for new operational conditions (He15K at T = 14.6 K, He23K-LP at T = 18.6 K, He23K-IP at T = 26.9 K, Ar50K at T = 76.0 K and Ar100K at 135.0 K) (see Figures S1-S5)). These new operational conditions, *i.e.* the required total pressure in the *reservoir* (P_{res}) and in the reaction chamber (P_{ch}), are listed in Table S2 for all supersonic flows together with the resulting jet temperature. The flow ranges of CH_3CHO (F_{CH3CHO}) shown in Table S1 are those corresponding to the linear part of the second-order plots.

Table S1 Experimental conditions employed in the study of the CH_3CHO+OH reaction.

T / K	% He	% Ar	% N_2	n / 10^{16} cm^{-3}	F_{buffer} / slpm	F_{CH3CHO} / sccm	F_{H2O2} / sccm	f_{CH3CHO} / 10^{-3}	[CH_3CHO] / 10^{13} cm^{-3}
11.7 ± 0.7	100			6.88 ± 0.62	4.71 – 4.87	5.0 – 63.1	99.1	11	0.078 – 0.979
13.0 ± 0.7	100			6.41 ± 0.55	3.54 – 3.65	5.0 – 97.4	99.1	6 – 11	0.096 – 1.06
14.6 ± 1.0	100			4.98 ± 0.51	2.67 – 2.79	9.9 – 97.4	99.1	6	0.112 – 1.07
18.6 ± 0.6	100			5.53 ± 0.25	4.45 – 4.57	5.0 – 97.4	61.8	6	0.038 – 0.743
21.1 ± 0.6	100			3.37 ± 0.15	5.05 – 5.29	60.0 – 235.5	33.9	10	0.399 – 1.56
22.5 ± 0.7	100			7.43 ± 0.32	9.56 – 10.24	60.2 – 633.1	80.5	5	0.211 – 2.22
21.7 ± 1.4	100			16.7 ± 1.6	9.31 – 11.67	15.2 – 143.6	19.3 – 99.1	8 – 12	0.326 – 1.76
26.9 ± 1.1	91		9	4.08 ± 0.26	4.19 – 4.33	5.0 – 91.0	99.1	26	0.122 – 2.24
36.2 ± 1.2	100			17.7 ± 0.9	14.47 – 15.30	60.2 – 677.1	52.5	5	0.338 – 4.54
45.3 ± 1.3	20		80	4.23 ± 0.28	1.34 – 1.51	31.0 – 137.9	19.4	8	0.652 – 2.93
50.5 ± 1.6			100	1.50 ± 0.12	0.81 – 1.27	56.4 – 433.4	17.2	2	0.161 – 1.25
51.6 ± 1.7 [a]			100	4.17 ± 0.35	11.94 – 12.20	39.5 – 222.4	72.7	26 – 51	0.346 – 1.95
49.9 ± 1.4	74		26	8.33 ± 0.41	3.57 – 4.15	60.1 – 587.6	12.8	4	0.474 – 4.62
52.1 ± 0.5		100		19.5 ± 0.3	4.50 – 4.72	53.2 – 183.6	15.6	1	0.132 – 0.455
64.2 ± 1.7 [a]			100	2.24 ± 0.15	3.52 – 3.95	56.1 – 388.1	17.2	30	0.954 – 6.64
64.1 ± 1.6	20		80	4.63 ± 0.27	1.78 – 1.97	17.1 – 143.3	7.5 – 10.3	9	0.363 – 3.05
64.4 ± 0.6		70	30	17.4 ± 0.3	3.33 – 3.41	6.6 – 497.0	16.0 – 44.5	1 – 5	0.131 – 1.09
76.0 ± 0.8		40	60	15.0 ± 0.3	2.69 – 3.02	35.5 – 307.7	19.6	3	0.296 – 2.56
89.5 ± 0.6			100	18.2 ± 0.3	6.42 – 6.93	56.4 – 474.9	19.6	3	0.174 – 5.64
107.0 ± 0.5			100	4.90 ± 0.06	0.66 – 1.17	56.4 – 474.9	2.9	3 – 5	0.652 – 5.66
106.0 ± 0.6		100		14.0 ± 0.1	1.33 – 1.66	62.5 – 322.6	9.8	3	1.63 – 8.35
115.3 ± 1.1		100		9.58 ± 0.14	0.80 – 0.97	11.3 – 125.9	20.1	21	2.33 – 27.1
136.1 ± 0.8			100	24.9 ± 0.4	4.58 – 5.04	56.3 – 474.2	38.1	10	2.73 – 22.9
135.0 ± 0.8			100	29.4 ± 0.5	4.45 – 6.05	7.3 – 71.5	28.8	46	1.56 – 16.5
158.8 ± 0.6			100	7.40 ± 0.07	0.51 – 1.02	56.3 – 474.2	19.6	10	3.99 – 34.6
177.5 ± 1.2			100	6.71 ± 0.11	0.25 – 0.68	55.9 – 427.9	14.9	10	5.29 – 41.1

[a] Continuous flow conditions. Slpm, standard litres per minute; sccm, standard cubic centimetres per minute.

Table S2 Operational conditions of the Laval nozzles employed in this work and the resulting jet temperature.

P_{res} / mbar	P_{ch} / mbar	T / K
366.48	0.117	11.7 ± 0.7
280.16	0.117	13.0 ± 0.7
188.74	0.110	14.6 ± 1.0
147.28	0.150	18.6 ± 0.6
73.88	0.125	21.1 ± 0.6
147.76	0.280	22.5 ± 0.7
337.21	0.620	21.7 ± 1.4
78.47	0.191	26.9 ± 1.1
173.32	1.10	36.2 ± 1.2
132.23	0.295	45.3 ± 1.3
52.12	0.120	50.5 ± 1.6
136.24	0.279	51.6 ± 1.7 [a]
86.00	0.620	49.9 ± 1.4
110.15	1.50	52.1 ± 0.5
41.67	0.183	64.2 ± 1.7 [a]
65.47	0.450	64.1 ± 1.6
112.60	1.670	64.4 ± 0.6
107.96	1.660	76.0 ± 0.8
151.59	2.370	89.5 ± 0.6
26.12	0.790	107.0 ± 0.5
27.09	2.515	106.0 ± 0.6
16.16	1.964	115.3 ± 1.1
71.99	5.20	136.1 ± 0.8
86.69	6.00	135.0 ± 0.8
14.37	1.961	158.8 ± 0.6
9.97	2.00	177.5 ± 1.2

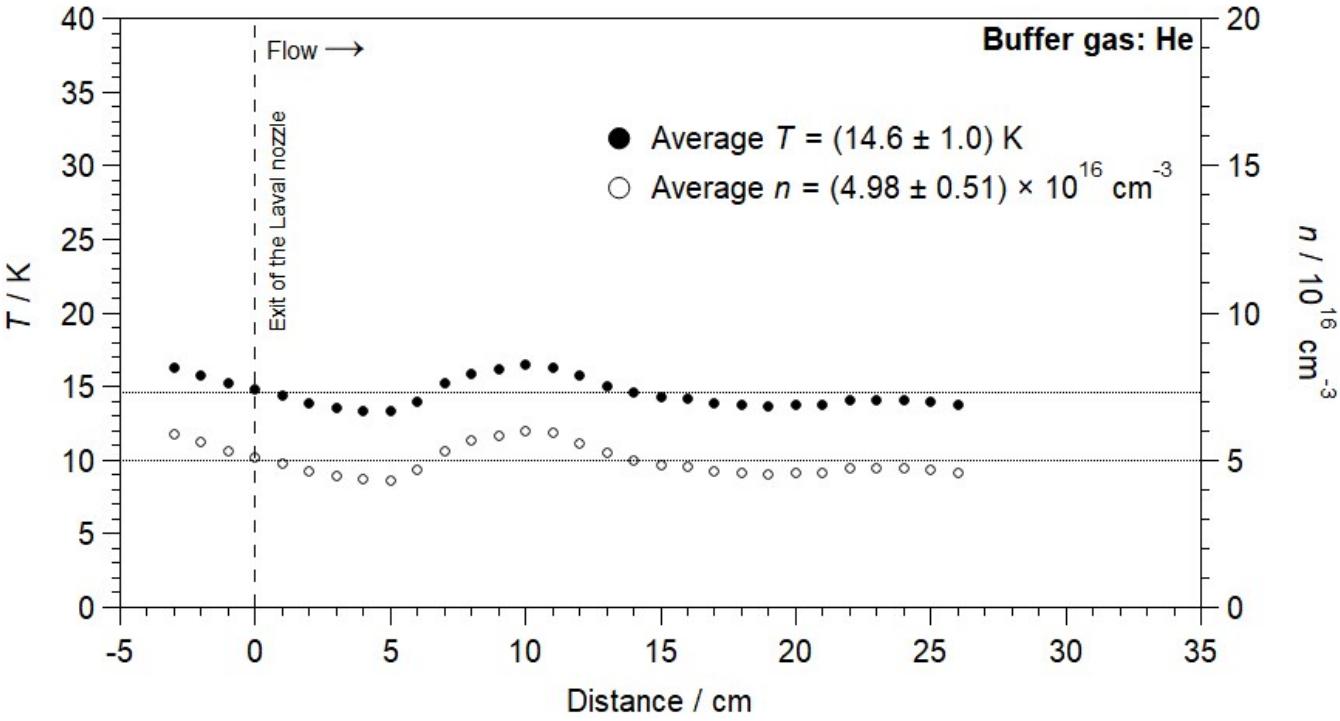

Figure S1 The spatial profile of temperature and gas density in the jet using the He15K nozzle.

[a] Continuous flow conditions.

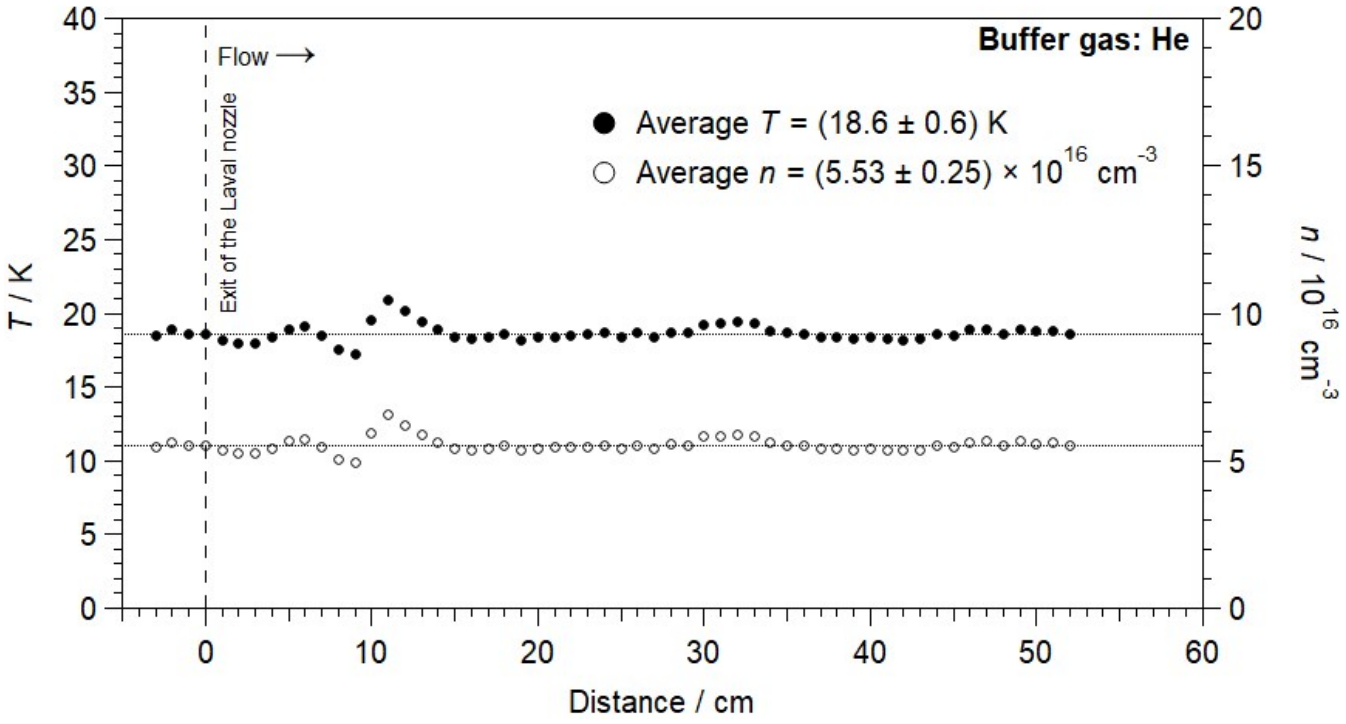

Figure S2 The spatial profile of temperature and gas density in the jet using the He23K-LP nozzle.

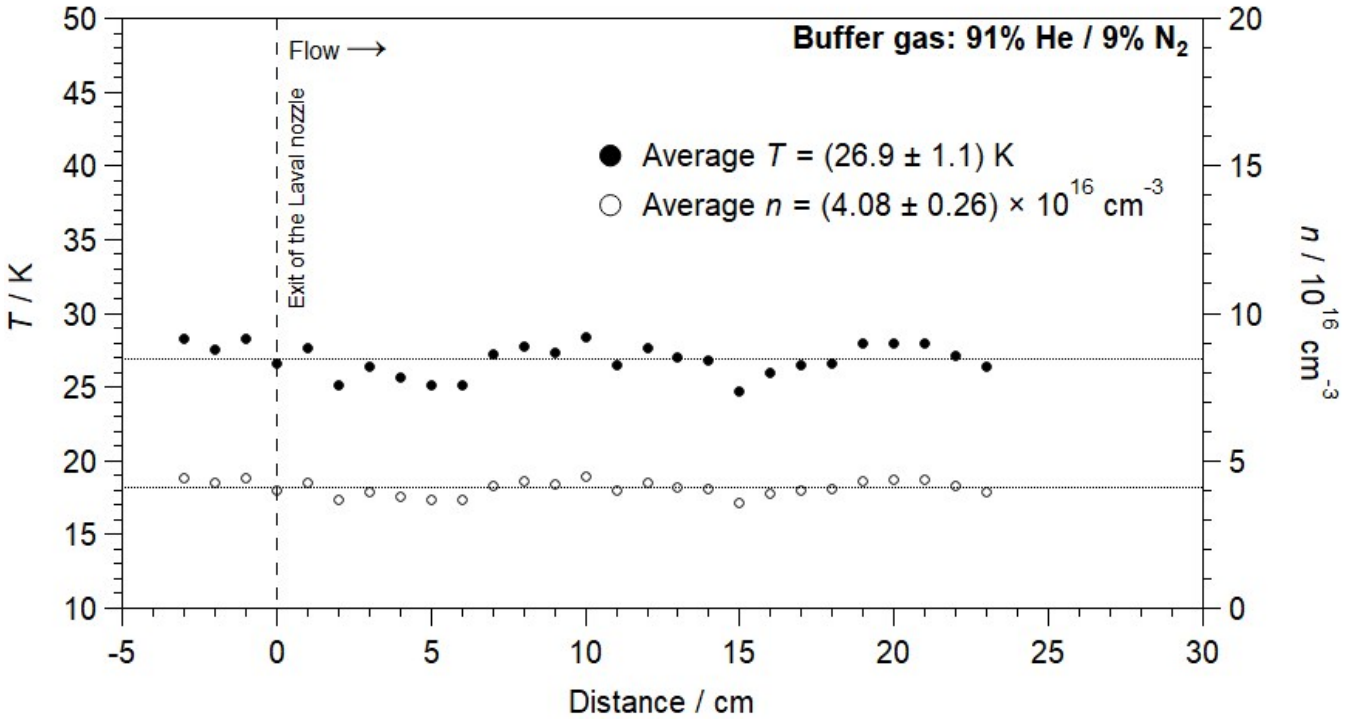

Figure S3 The spatial profile of temperature and gas density in the jet using the He23K-IP nozzle.

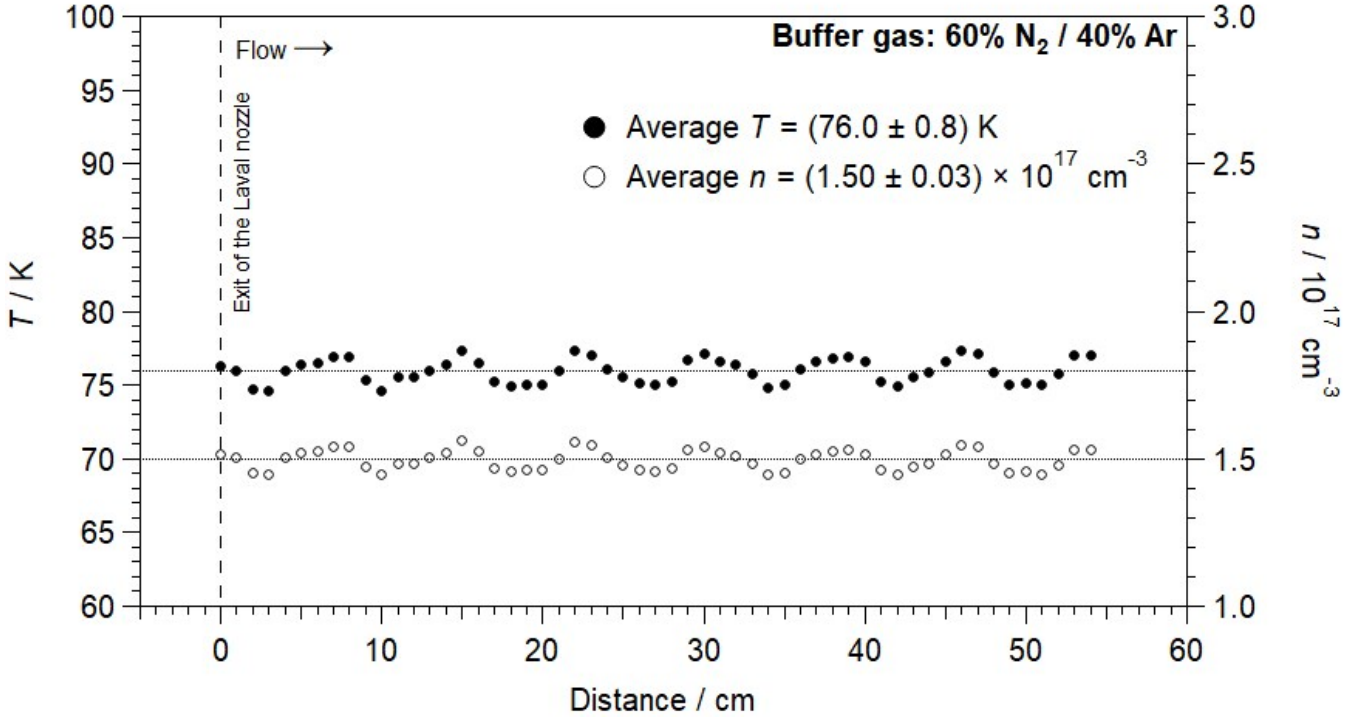

Figure S5 The spatial profile of temperature and gas density in the jet using the Ar50K nozzle.

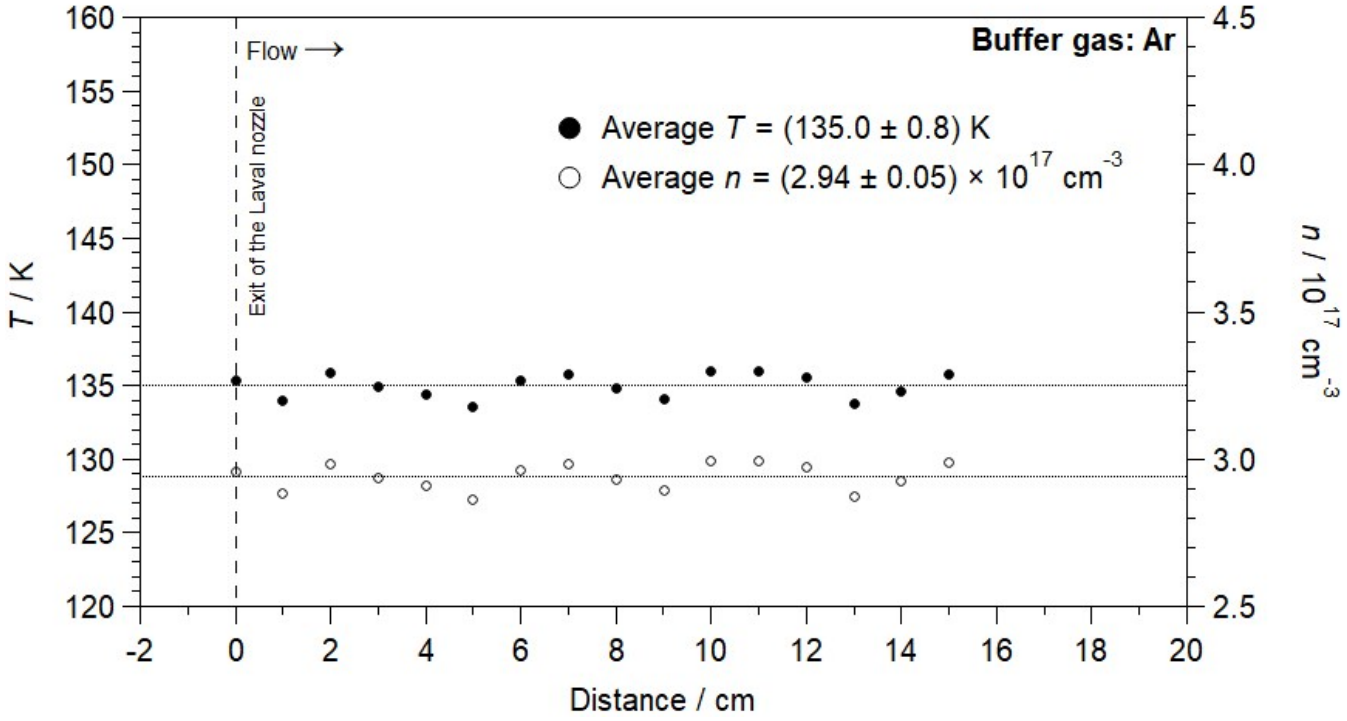

Figure S4 The spatial profile of temperature and gas density in the jet using the Ar100K nozzle.

Dimerization of CH_3CHO

In low temperature kinetic studies, clustering processes are favoured and occur in the timescale of the experiments when high concentrations of reagent (CH_3CHO in this work) are introduced in the system. The first step of a clustering process, the dimerization, has been widely reported in the literature.[2, 3, 5, 6, 9, 10] If the dimerization of CH_3CHO is occurring, the rate coefficient can be underestimated as the amount of "free" acetaldehyde would be much lower. However, the initial [CH_3CHO] employed in this work are low enough to ensure that the dimerization process is not affecting the measured $k(T)$. We usually performed the kinetic studies in a wider concentration range than those presented in Table S1 to identify the onset for dimerization, i.e., the concentration beyond which the bimolecular plots (as those shown in Fig. S6 for 11.7 and 21.7 K) start to present a downward curvature. Once this onset is identified, all kinetic experiments at a fixed temperature were carried out in the linear part of the k' *versus* [CH_3CHO] plots and $k(T)$ is obtained from the slope of such a plot. In Figure S6, the red circles correspond to kinetic data in the curved zone, where dimerization interferes in the determination of $k(T)$. These data were disregarded in the kinetic analysis and more experiments in the suitable concentration range were performed (listed in Table S1).

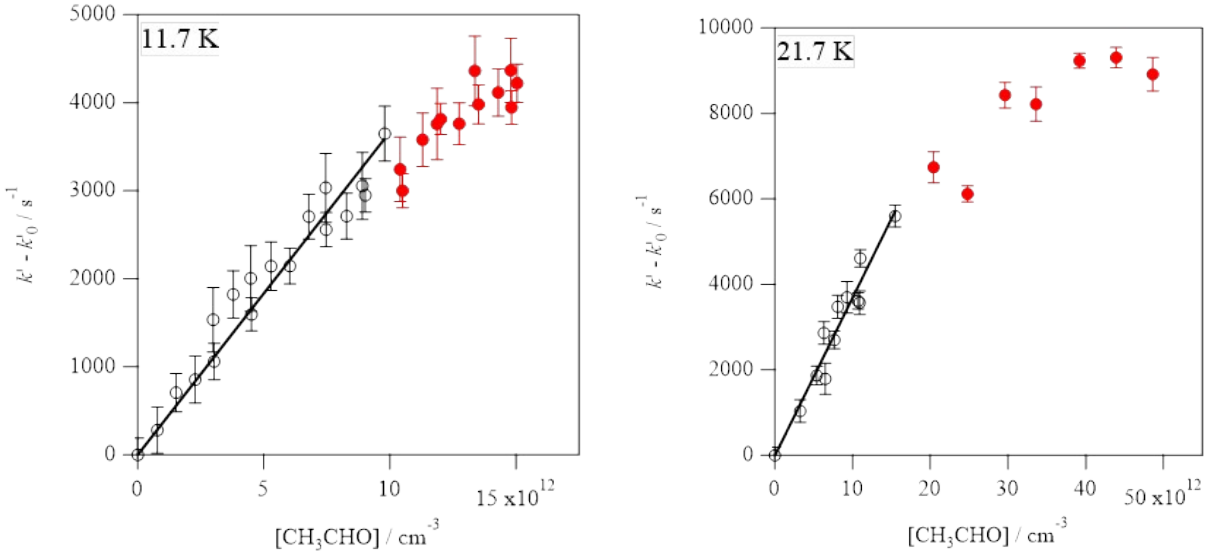

Figure S6. Examples of downward curvature in the bimolecular plots at 11.7 K and 21.7 K.

References

1. S. Blázquez, D. González, A. García-Sáez, M. Antiñolo, A. Bergeat, F. Caralp, R. Mereau, A. Canosa, B. Ballesteros, J. Albaladejo and E. Jiménez, *ACS Earth and Space Chemistry*, 2019, **3**, 1873-1883.
2. A. J. Ocaña, S. Blázquez, A. Potapov, B. Ballesteros, A. Canosa, M. Antiñolo, L. Vereecken, J. Albaladejo and E. Jiménez, *Physical Chemistry Chemical Physics*, 2019, **21**, 6942-6957.
3. M. Antiñolo, M. Agúndez, E. Jiménez, B. Ballesteros, A. Canosa, G. El Dib, J. Albaladejo and J. Cernicharo, *The Astrophysical Journal*, 2016, **823**, 25.
4. A. J. Ocaña, S. Blázquez, B. Ballesteros, A. Canosa, M. Antiñolo, J. Albaladejo and E. Jiménez, *Physical Chemistry Chemical Physics*, 2018, **20**, 5865-5873.
5. A. J. Ocaña, E. Jiménez, B. Ballesteros, A. Canosa, M. Antiñolo, J. Albaladejo, M. Agúndez, J. Cernicharo, A. Zanchet, P. Del Mazo, O. Roncero and A. Aguado, *The Astrophysical Journal*, 2017, **850**, 28.
6. E. Jiménez, M. Antiñolo, B. Ballesteros, A. Canosa and J. Albaladejo, *Physical Chemistry Chemical Physics*, 2016, **18**, 2183-2191.
7. E. Jiménez, B. Ballesteros, A. Canosa, T. M. Townsend, F. J. Maigler, V. Napal, B. R. Rowe and J. Albaladejo, *Review of Scientific Instruments*, 2015, **86**, 045108.
8. A. Canosa, A. J. Ocaña, M. Antiñolo, B. Ballesteros, E. Jiménez and J. Albaladejo, *Experiments in Fluids*, 2016, **57**, 152.
9. S. Hamon, S. D. Le Picard, A. Canosa, B. R. Rowe and I. W. M. Smith, *The Journal of Chemical Physics*, 2000, **112**, 4506-4516.
10. I. R. Sims, J. L. Queffelec, A. Defrance, C. Rebrion-Rowe, D. Travers, P. Bocherel, B. R. Rowe and I. W. M. Smith, *The Journal of Chemical Physics*, 1994, **100**, 4229-4241.